Mechanics of Advanced Composite Structures 12 (2025), Serial Number 24, 235 – 248

Mechanics of Advanced Composite Structures

Journal homepage: https://macs.semnan.ac.ir/

Semnan University

ISSN: 2423-7043

Research Article

Two-dimensional Elasticity Solutions For Analyzing Free Vibration Of Functionally Graded Porous Beams

Quoc-Cuong Le [a], Ba-Duy Nguyen [b*]

[a] *Institute of Engineering and Technology, Thu Dau Mot University, Thu Dau Mot City, Vietnam*

[b] *Faculty of Architecture, Thu Dau Mot University, Thu Dau Mot City, Vietnam*

ARTICLE INFO

Article history:

Received: 2023-12-08

Revised: 2024-07-26

Accepted: 2024-08-12

Keywords:

Vibration;

Functionally graded porous beams;

Two-Dimensional elasticity;

Porosity distributions.

ABSTRACT

A novel two-dimensional elasticity solution is presented in this paper, specifically designed for studying the vibration of functionally graded porous (FGP) beams. The kinetics of the beam are defined by two-dimensional elasticity theory, and Lagrange's equations are used to derive the governing equations of motion. The Ritz method devises the expansion of displacement variables in polynomial and trigonometric series in the thickness and axial directions. Furthermore, microvoids can emerge as a result of technical issues during the manufacture of functionally graded materials (FGMs), leading to the development of porosities. The porosity distribution functions, one for three porosity distributions: uniform porosity (UP), non-uniform porosity-I (NUP-I), and non-uniform porosity-II (NUP-II), are considered in the problem. This study investigates the impact of the gradation exponents (p) in the z-direction, the slenderness ratio (L/h), the distribution of porosity, the porosity coefficient (e), and various boundary conditions on the natural frequencies. A comparison with the findings from higher-order shear deformation theory (HSDT) validated the accuracy and effectiveness of the proposed methodology.

1. Introduction

In recent years, there has been a general upward trend in the number of applications that use porous structures in several sectors, such as civil engineering for the creation of protective layers, space engineering for the development of lightweight aircraft, and biomedical engineering for the creation of implants and scaffolds [1-4]. Functionally graded porous (FGP) structures [5 - 14] have captured the interest of several researchers because of their diverse range of applications. Vibration, buckling, and bending behavior of porous beams are all interesting and challenging problems in this field.

Numerous theories have been proposed to explore the behavior of FGP beams. Classical beam theory (CBT) and first-order beam theory (FBT) were very popular in the analysis. Eltaher et al. [15] conducted a CBT-based analysis of the vibration and bending behaviors of FGP nanobeams. The analysis of the linear and nonlinear vibrations of FGP beams was conducted by Wattanasakulpong et al. [16], who applied computational beam theory (CBT) methodology to the analysis of the linear and nonlinear vibrations of FGP beams. Based on CBT and the nonlocal strain gradient theory, Hieu et al. [17] used CBT and the nonlocal strain gradient theory to investigate how an FGP microbeam resting on an elastic base can cause buckling and

* **Corresponding author.**
E-mail address: duynb@tdmu.edu.vn

Cite this article as:

Le, Q. and Nguyen, B., 2025. Two-dimensional Elasticity Solutions For Analyzing Free Vibration Of Functionally Graded Porous Beams. *Mechanics of Advanced Composite Structures*, 12(1), pp. 235-248.

https://doi.org/10.22075/MACS.2024.32009.1594

nonlinear free vibration. Because shear deformation is not considered, CBT can only be used for thin beams. Researchers created FBT to account for the significant shear deformation in moderate and thick beams. Chen et al. [18] performed elastic buckling and static bending tests on FGP beams that can be deformed in shear using the Timoshenko beam theory. Kitipornchai et al. [19] found the free frequency and critical buckling stress of FGP beams that were strengthened with graphene platelets. Jing_Zhao et al. [20] established a modified series solution utilizing FBT to analyze the free vibrations of moderately thick FGP deep curved and straight beams. Pham et al. [21] developed an improved first-order beam element that uses the neutral surface location to analyze the bending of FGP beams. Using analytical, finite element, and artificial neural network techniques, Turan et al. [22] examined the free vibration and buckling of functionally graded porous beams under various boundary conditions. Evidently, FBT is being used more frequently to analyze the behavior of FGP beams; nevertheless, determining the necessary shear correction factor presents a challenge. HBTs can be used to solve FGP beams. Adıyaman [23] investigated the free vibration analysis of an FGP beam using higher-order shear deformation theory (HSDT). Suppakit Eiadtrong et al. [24] devised the thermal vibration of FGP beams using HSDT with classical and non-classical boundary conditions by employing a modified Fourier method. Using higher-order theories, Mahmoud Askari [25] performed vibration analysis of coupled transverse and shear piezoelectric functionally graded porous beams. Nguyen et al. [26] presented a simple two-variable shear deformation theory for the bucking, bending, and vibration behaviors of FGP beams. With the aid of the Chebyshev collocation method and HSBT, Wattanasakulpong et al. [27] analyzed the free vibration of FGP beams. Bin Qin [28] presented an analysis of the free and forced vibrations of FGP straight beams under arbitrary boundary conditions using HSDT. Y. Shabani et al. [29] conducted an analytical solution for static buckling and free vibration analysis of bi-dimensional functionally graded (2D-FG) metal-ceramic porous beams.

Numerous techniques have been developed for analyzing FGP beams, with the finite element method (FEM) being the most prevalent. The vibration of porous beams was analyzed by Rjoub and Hamad [30] using the Transfer Matrix Method. To analyze the buckling, static, and dynamic behaviors of porous graphene-reinforced curved beams, Anirudh et al. [31] developed the FEM. Di Wu et al. [32] used the FEM to conduct calculations on FGP beam-type structures, specifically focusing on both free and forced vibrations. Mesbah et al. [33] used FEM to analyze the behavior of FGP beams under circumstances of free vibration and buckling. M. Turan [34] introduced a novel higher-order FEM for analyzing the static behavior of functionally graded porous beams in two directions.

In addition, numerous scientists have been intrigued by the Ritz method to understand the behavior of FGP beams. D. Chen [35] investigated the free and forced vibrations of shear-deformable FGP beams using the Ritz method and the Newmark β approach. A modified Fourier series technique based on the Ritz method was employed by Zhao et al. [36] to analyze the vibration of deep-curved FGP beams. Bin Qin [28] developed a Jacobi-Ritz approach to analyze the free and forced vibrations of FGP straight beams with arbitrary boundary conditions using HSDT. Nguyen et al. [37] introduced a Legendre-Ritz method to solve the bending, buckling, and free vibration characteristics of FGP beams supported by an elastic foundation. Hung et al. [38] conducted a nonlinear bending analysis of beams made of FG porous material reinforced with graphene platelets. The analysis was performed using the Ritz approach, which considered several boundary conditions.

Elasticity theory is another viable option because it considers thickness-wise deformation. Sankar [39] proposed an elasticity solution for beams with functionally graded material properties. Yang et al. [40] introduced the elasticity solutions of the equilibrium equations in the plate and the traction boundary conditions on the faces of the plates. A. Singh et al. [41] developed a precise two-dimensional (2D) elasticity solution for an axially functionally graded (FG) beam with an arbitrary support. Miao et al. [42] completed a study on a two-dimensional elasticity model to analyze the bending and free vibration of laminated graphene-reinforced composite beams. Peng Wu et al. [43] presented exact solutions for simply supported multilayer functionally graded (FG) beams with viscoelastic interlayers to forecast their time-dependent mechanical characteristics. For curved sandwich beams with FG-CNTRC face sheets and porous cores, Serajzadeh et al. [44] developed a two-dimensional low-velocity impact model. Amir Najibi et al. [45, 46] conducted two compelling experiments using 3D elasticity theory. The first study investigated the natural frequencies of a thick hollow cylinder using the 2D-FGM Mori-Tanaka scheme. The second study examined the natural frequencies of a bidirectional FG truncated thick hollow cone in three dimensions.

However, the applicability of exact solutions obtained using elasticity equations is restricted to basic geometries and particular boundary conditions. Thus, the development of a straightforward beam theory for structures composed of FGP materials will be beneficial. By juxtaposing the beam theory with the elasticity solutions, we can establish their validity. The exact solutions to the plane elasticity equations yield the stress and displacement fields. The preceding results of the FSBT [22] and HSBT [23, 47-49] are compared with the outcomes derived from the elasticity theory.

The primary aim of this study is to provide a two-dimensional elasticity solution for examining the natural vibration of FGP beams with three distinct porosity distributions: uniform porosity (UP), non-uniform porosity-I (NUP-I), and non-uniform porosity-II (NUP-II). An in-depth analysis and discussion are conducted on the impact of boundary conditions, the span-to-height ratio, the porous distribution pattern, and the porosity coefficient. The undisclosed findings are showcased as a benchmark for future investigations.

2. Theoretical Formulation

2.1. Functionally Graded Porous Beams

The diagram in Figure 1 illustrates a PFG beam that possesses a rectangular cross-section with dimensions (b x h) and a linear length represented by the symbol L.

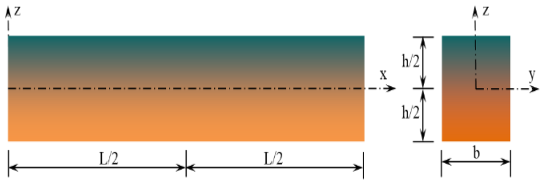

Fig. 1. Geometry of the FGP beam

The FGP beams have a consistent range of characteristics that are proportional to the volume of the various isotropic metal and ceramic components. The following power-law expression illustrates the useful properties of the FGP beams [4, 23]:

$$\zeta(z)=\zeta_m+(\zeta_c-\zeta_m)\left(\frac{2z+h}{2h}\right)^p-\frac{e}{2}f_e(z)(\zeta_c+\zeta_m) \qquad (1)$$

where p is a power-law index, e represents the porosity coefficient, ζ_c and are the mass density ρ, Young's modulus E, and shear modulus, respectively. $f_e(z)$ is a function that depicts the distribution of the void along the thickness of the beam.

In this paper, three porosity distributions (UP, NUP-I and NUP-II) shown in Fig. 2 are considered as follows:

UP: $$f_e(z)=1 \qquad (2a)$$

NUP-I: $$f_e(z)=1-\frac{2|z|}{h} \qquad (2b)$$

NUP-II: $$f_e(z)=\sin\left(\frac{|z|}{h}\pi\right) \qquad (2c)$$

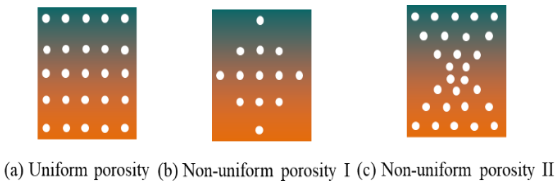

Fig. 2. Cross-sectional beam for various distribution functions

2.2. Kinematics

By and at the position (x, z) of the beam, respectively, denote the axial and transverse displacements. The relationships between the linear displacement and strain of the beam are:

$$\varepsilon_x=u_{,x}, \quad \varepsilon_z=w_{,z}, \quad \gamma_{xz}=u_{,z}+w_{,x} \qquad (3)$$

where the comma denotes a distinction in relation to the subscript that follows the coordinates. Given the estimated plan stress in the beam plane (x, z), i.e. $\sigma_y=\sigma_{yz}=\sigma_{xy}=0$.

In a generalized coordinate system, the elastic constitutive equation is written as:

$$\begin{Bmatrix}\sigma_x\\ \sigma_z\\ \sigma_{xz}\end{Bmatrix}=\begin{bmatrix}A_{11} & A_{13} & 0\\ A_{13} & A_{33} & 0\\ 0 & 0 & A_{55}\end{bmatrix}\begin{Bmatrix}\varepsilon_x\\ \varepsilon_z\\ \gamma_{xz}\end{Bmatrix} \qquad (4)$$

The Coefficients of elastic stiffness of FGP beams, namely those pertaining to in-plane and out-of-plane reductions, are represented as A_{11}, A_{33}, A_{13}, and A_{55}. The stiffness coefficients corresponding to position z are given as follows:

$$A_{11}(z)=A_{33}(z)=\frac{E(z)}{1-\nu^2}$$

$$A_{13}(z)=\frac{\nu E(z)}{1-\nu^2} \qquad (5)$$

$$A_{55}(z)=\frac{E(z)}{2(1+\nu)}$$

The constant ν in this study represents Poisson's ratio and is assumed to have a value of 0.3.

2.3. Lagrange's Formulas

The Lagrangian function is used to derive the kinetic equations:

$$\Pi = U - K \tag{6}$$

The U strain energy of the system can be represented as

$$\begin{aligned} U &= \frac{1}{2}\int_V \left(\sigma_x \varepsilon_x + \sigma_z \varepsilon_z + \sigma_{xz}\gamma_{xz}\right) dV \\ &= \frac{1}{2}\int_V \Big[A_{11}u_{,x}^2 + 2A_{13}u_{,x}w_{,z} + A_{33}w_{,z}^2 \\ &\qquad + A_{55}\left(u_{,z}^2 + 2u_{,z}w_{,x} + w_{,x}^2\right)\Big] dV \end{aligned} \tag{7}$$

The symbol for kinetic energy is K.

$$K = \frac{1}{2}\int_V \rho\left(\dot{u}^2 + \dot{w}^2\right) dV \tag{8}$$

where ρ is the layer mass density, and the dot-superscript convention represents differentiation with respect to time t.

By substituting Eqs. (7) and (8) into Eq. (6), the Lagrangian function becomes:

$$\begin{aligned} \Pi &= \frac{1}{2}\int_V \Big[A_{11}u_{,x}^2 + 2A_{13}u_{,x}w_{,z} + A_{33}w_{,z}^2 \\ &\qquad + A_{55}\left(u_{,z}^2 + 2u_{,z}w_{,x} + w_{,x}^2\right)\Big] dV \\ &\quad - \frac{1}{2}\int_V \rho\left(\dot{u}^2 + \dot{w}^2\right) dV \end{aligned} \tag{9}$$

2.4. Two-directional Ritz Solution

The Ritz technique provides a set of approximations for the axial and transverse displacements of the FGP beams at a specific position (x, z).

$$u(x,z,t) = \sum_{r=1}^{R}\sum_{s=1}^{S} \alpha_{rs}(x,z)u_{rs}(t) \tag{10a}$$

$$w(x,z,t) = \sum_{r=1}^{R}\sum_{s=1}^{S} \beta_{rs}(x,z)w_{rs}(t) \tag{10b}$$

where u_{rs}, w_{rs} are the displacements that need to be computed, and $\alpha_{rs}(x,z)$, $\beta_{rs}(x,z)$ are the bidirectional shape functions illustrated in table 1 and 2, which consist of a trigonometric function on the x-axis and a polynomial function on the z-axis.

Table 1. Approximation functions of the beams

BC	$\alpha_{rs}(x,z)$	$\beta_{rs}(x,z)$
S-S	$\cos\left(\frac{r\pi x}{L}\right)z^{s-1}$	$\sin\left(\frac{r\pi x}{L}\right)z^{s-1}$
C-F	$\sin\left(\frac{(2r-1)\pi x}{2L}\right)z^{s-1}$	$\left(1-\cos\left(\frac{(2r-1)\pi x}{2L}\right)\right)z^{s-1}$
C-C	$\sin\left(\frac{2r\pi x}{L}\right)z^{s-1}$	$\sin^2\left(\frac{r\pi x}{L}\right)z^{s-1}$

Table 2. Essential boundary conditions of the beams

BC	x = 0	x = L
S-S	$w=0$	$w=0$
C-F	$u=w=w_{,x}=0$	
C-C	$u=w=w_{,x}=0$	$u=w=w_{,x}=0$

Substituting Eqs. (10a), (10b) into Eq. (9), along with Lagrange's equations, yields the governing equations of motion:

$$\frac{\partial \Pi}{\partial q_{rs}} - \frac{d}{dt}\frac{\partial \Pi}{\partial \dot{q}_{rs}} = 0 \tag{11}$$

with q_{rs} symbolizing the importance of (u_{rs}, w_{rs}), resulting in

$$\left(\begin{bmatrix} \boldsymbol{K}^{11} & \boldsymbol{K}^{12} \\ {}^{T}\boldsymbol{K}^{12} & \boldsymbol{K}^{22} \end{bmatrix} - \omega^2 \begin{bmatrix} \boldsymbol{M}^{11} & \boldsymbol{0} \\ \boldsymbol{0} & \boldsymbol{M}^{22} \end{bmatrix}\right)\begin{Bmatrix} \boldsymbol{u} \\ \boldsymbol{w} \end{Bmatrix} = \begin{Bmatrix} \boldsymbol{0} \\ \boldsymbol{0} \end{Bmatrix} \tag{12}$$

where $\boldsymbol{K}$ and $\boldsymbol{M}$ are the matrices of stiffness and mass, respectively, and their components are provided by

$$\begin{aligned} K_{rspq}^{11} &= \int_0^L\int_{-h/2}^{h/2} A_{11}\alpha_{rs,x}(x,z)\alpha_{pq,x}(x,z)dxdz \\ &\quad + \int_0^L\int_{-h/2}^{h/2} A_{55}\alpha_{rs,z}(x,z)\alpha_{pq,z}(x,z)dxdz \\ K_{rspq}^{12} &= \int_0^L\int_{-h/2}^{h/2} A_{13}\alpha_{rs,x}(x,z)\beta_{pq,z}(x,z)dxdz \\ &\quad + \int_0^L\int_{-h/2}^{h/2} A_{55}\alpha_{rs,z}(x,z)\beta_{pq,x}(x,z)dxdz, \\ K_{rspq}^{22} &= \int_0^L\int_{-h/2}^{h/2} A_{33}\beta_{rs,z}(x,z)\beta_{pq,z}(x,z)dxdz \\ &\quad + \int_0^L\int_{-h/2}^{h/2} A_{55}\beta_{rs,x}(x,z)\beta_{pq,x}(x,z)dxdz, \\ M_{rspq}^{11} &= \int_0^L\int_{-h/2}^{h/2} \rho(z)\alpha_{rs}(x,z)\alpha_{pq}(x,z)dxdz, \\ M_{rspq}^{22} &= \int_0^L\int_{-h/2}^{h/2} \rho(z)\beta_{rs}(x,z)\beta_{pq}(x,z)dxdz \end{aligned} \tag{13}$$

Finally, upon solving Eq. (13), the vibration responses of the PFG beams can be obtained.

3. Mathematical Outcomes and Discussions

The numerical results are based on the assumption that the bottom of the beam is composed of metal, whereas the top of the beam comprises ceramic. The parameters of the materials used in the solutions are detailed in Table 3. To obtain these results, three different boundary conditions of the beam were considered: Simply supported (S-S), clamped-clamped (C-C), and clamped-free (C-F). It should be noted that the results normalized fundamental frequencies (NFF) are standardized to the following values:

$$\bar{\omega} = \frac{\omega L^2}{h}\sqrt{\frac{\rho_m}{E_m}} \tag{14}$$

where the subscript m indicates the metal-related characteristics.

Table 3. Material property

Material	***E*(GPa)**	**ρ (kg/m³)**	ν
Ceramic (Al_2O_3)	380	3960	0.3
Metal (Al)	70	2702	0.3

3.1. Convergence Study

This particular investigation focuses on a NUP-I beam with the following parameters: L/h = 5, p = 1, and e = 0.1 to evaluate the convergence properties. Table 4 presents the NFF of the FGP beams for various boundary conditions. The values Nx and Nz represent the number of series along the x and z axes, respectively, as a function of the NFF. The solutions demonstrate an impressive speed of convergence in the x-direction, where a significant number of series are involved in this specific dimension. The convergence of the NFF may be observed at a specific value of N_x, which is determined to be 12 based on the various boundary conditions. Nevertheless, as the number of series in the z-direction increases, the NFF decreases, resulting in the beam displaying softening characteristics. For further verification, N_x = 12 and N_z = 4 will be used as examples in the impending paper.

3.2. Free Vibration Analysis

Validation is an essential procedure to ascertain the precision and dependability of the results. Table 5 shows the different FGP beams that were tested. This study examines changes in the power-law index, span-to-height ratio, porosity ratio, porosity distribution type, and boundary conditions. The aforementioned values were compared with the outcomes derived using Turan [22] and Gökhan [23], which implemented HSBT and FEM. Hadji et al. [47] used the Navier-type solution method and the new HSBT. It is evident that the present findings are consistent with those previously reported. The proposed theory's Eq. 3 posits that deformation along the beam's thickness causes the stress. Previous theoretical bases (CBT, FBT, and HSBT) typically did not discuss this issue. Therefore, the frequencies observed in the current investigation exhibit only minor deviations from those reported in previous studies.

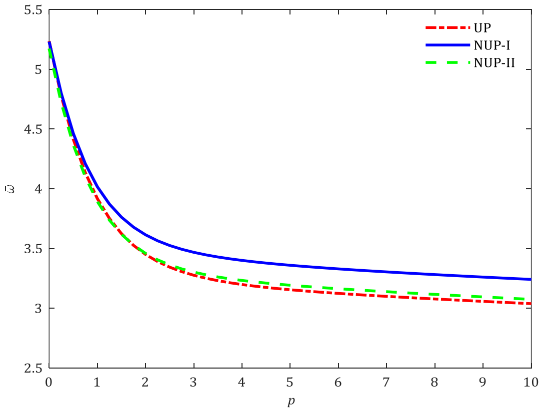

Fig. 3. NFF (S - S, e = 0.1, L/h = 5) of various porosity distribution types with respect to the power law index p

An additional validation of the NFF acquired in the research is presented in Table 6 when the perfect cross-section is compared to the frequencies specified by Turan et al. [22], Nguyen et al. [48], Vo et al. [49], and Gökhan [23] for various p and boundary conditions. Particularly for Turan's research results, the errors in percent are between 0.012% and 0.225% in the case of L/h = 5, while for L/h = 20, the two research results are almost identical; the difference is only 0.02 for UP and from 0.02% to 0.064% for NUP-I. Analysis of the data presented in Table 6 reveals that the frequencies observed in the current investigation exhibit only minor deviations (0.008% to 1.304%) from those reported in previous studies.

An S–S beam (L/h = 5 and e = 0.1) is considered from the UP, NUP-I, and NUP-2 series to investigate the effect of porosity distribution patterns on the NFF. The NFF of the UP, NUP-I, and NUP-2 beams is illustrated in Figure 3 as an expression of p. The NFF of all beams, when normalized, demonstrates a significant decrease throughout the region of $0 \le p < 2$. However, this reduction is less pronounced for p-values greater than 2. Furthermore, the NUP-I beams demonstrate the greatest NFF, whereas the UP beams showcase the lowest values.

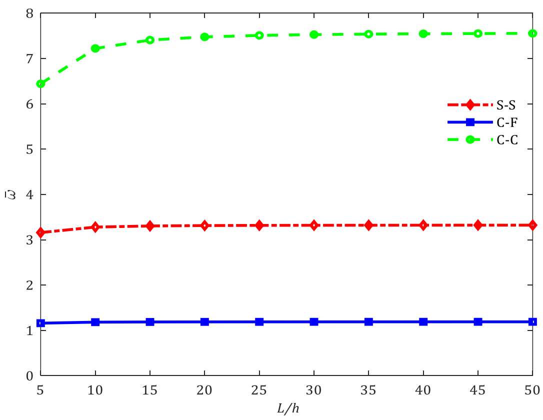

Fig. 4. NFF (p = 2, e = 0,2) of UP beams with various boundary conditions

Figure 4 shows the NFF of UP beams (p = 2, e = 0,2) in relation to the L/h ratio under various boundary conditions. The NFF for the C-C beams demonstrated substantial increases as the L/h ratio increased, whereas these increases were comparatively negligible for the S-S and C-F beams. It is worth noting that NFF is highest in C-C beams and lowest in C-F beams.

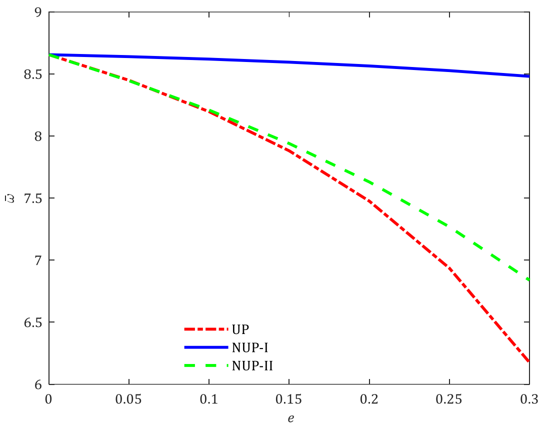

Fig. 5. NFF of C - C beams (p=2, L/h = 5) with respect to porosity ratio

Figure 5 illustrates the investigation into the impact of the porosity ratio on the NFF of the C-C beams (L/h = 5 and p = 2). With regard to vibration behavior, it is evident that the NFF for the UP and NUP-II beams decreases considerably as the porosity ratio increases, whereas the NUP-I beams experience minimal change. As the porosity ratio increases, both stiffness and inertial mass decrease. The reduction in rigidity is more conspicuous in the case of the UP and NUP-II beams compared to the reduction in inertial mass. However, this distinction is trivial concerning the NUP-I beams.

To validate the outcomes, an assortment of FGP beams were examined, each possessing distinct characteristics including power-law index, span-to-height ratio, porosity ratio, porosity distribution type, and boundary conditions. Tables 7, 8, and 9, respectively, display the NFF of the S-S, C-C, and C-F beams. The NFF increases as e increases for p = 0, as shown in the tables above. However, for p > 0, an increase in e decreases in frequencies. By detailing the corresponding changes in the shear and elastic moduli and the density, Eq. 1 provides a straightforward explanation of the NFF change. Nevertheless, as porosity increases, the proportional change in density outweighs the relative changes in the elastic modulus and shear modulus around p = 0. Because the global stiffness matrix $\boldsymbol{K}$ comprises the elastic modulus; and shear modulus, and the global mass matrix $\boldsymbol{M}$ comprises the density, the NFF increases as the porosity increases, as determined by Eq. 12. Nevertheless, for $p \geq 0.5$, the relative change in density is not reflected in the relative change in the elastic and shear moduli.

Furthermore, as porosity increases, so does NFF. NFF rises in direct proportion to L/h. The UP type experiences the greatest frequency shift with increased porosity, whereas the NUP-I type experiences the least. Moreover, in all three instances (UP, NUP-I, and NUP-II), the NFF of C-C continued to provide the highest value and the NFF of C-F the lowest value, even when the coefficients e and p grew simultaneously.

Table 4. Convergence analyses of the NFF of FGP beams (NUP-I, L/h = 5, p = 1, and e = 0.1)

BCs	Nz	Nx							
		2	**4**	**6**	**8**	**10**	**12**	**14**	**16**
S-S	1	15.8204	15.8204	15.8204	15.8204	15.8204	15.8204	15.8204	15.8204
	2	4.2058	4.2058	4.2058	4.2058	4.2058	4.2058	4.2058	4.2058
	3	4.0315	4.0315	4.0315	4.0315	4.0315	4.0315	4.0315	4.0315
	4	4.0167	4.0167	4.0167	4.0167	4.0167	4.0167	4.0167	4.0167
	5	4.0163	4.0163	4.0163	4.0163	4.0163	4.0163	4.0163	4.0163
	6	4.0163	4.0163	4.0163	4.0163	4.0163	4.0163	4.0163	4.0163
C-F	1	8.7113	8.3204	8.1832	8.1143	8.073	8.0456	8.0261	8.0115
	2	1.5466	1.5423	1.5413	1.5408	1.5406	1.5404	1.5403	1.5402
	3	1.5265	1.5030	1.4942	1.4896	1.4869	1.4851	1.4838	1.4828
	4	1.5228	1.4990	1.4901	1.4855	1.4828	1.4810	1.4798	1.4789
	5	1.5227	1.4990	1.4901	1.4855	1.4827	1.4809	1.4797	1.4788
	6	1.5227	1.4990	1.4900	1.4854	1.4826	1.4808	1.4795	1.4786
C-C	1	17.2098	16.5653	16.3291	16.2066	16.1316	16.081	16.0446	16.017
	2	8.6061	8.5084	8.4763	8.4601	8.4503	8.4437	8.4389	8.4354
	3	8.4275	8.2851	8.2321	8.2046	8.1879	8.1769	8.1690	8.1631
	4	8.2902	8.1464	8.0953	8.0699	8.0552	8.0456	8.0390	8.0341
	5	8.2885	8.1448	8.0934	8.0676	8.0522	8.0421	8.0349	8.0295
	6	8.2881	8.1436	8.0910	8.0643	8.0484	8.0379	8.0305	8.0250

Table 5. Comparison of the NFF found in this investigation with the frequencies reported in Turan et al. [22], Hadji et al. [47], and Gökhan [23] (S-S, p= 2)

L/h	Theory	UP			NUP-I		
		e = 0	e = 0.1	e = 0.2	e = 0	e = 0.1	e = 0.2
5	M. Turan [22]	3.6344	3.4496	3.1554	3.6344	3.6187	3.5949
	Hadji et al. [47]	3.6264	3.4418	3.1489	3.6264	3.6069	3.5785
	Gökhan [23]	3.5970	3.4050	3.1023	3.5970	3.5736	3.5405
	Outcome	3.6323	3.4500	3.1589	3.6323	3.6142	3.5868
10	M. Turan [22]	3.7929	3.5941	3.2789	3.7929	3.7790	3.7567
	Outcome	3.7921	3.5941	3.2797	3.7921	3.7776	3.7543
20	M. Turan [22]	3.8368	3.6340	3.3128	3.8368	3.8235	3.8017
	Hadji et al. [47]	3.8361	3.6335	3.3123	3.8361	3.8226	3.8004
	Gökhan [23]	3.8341	3.6308	3.3090	3.8341	3.8201	3.7975
	Outcome	3.8365	3.6340	3.3130	3.8365	3.8232	3.8013

Table 6. Comparison of NFF found in this investigation with the frequencies reported in Turan et al. [22], Nguyen et al. [48], Vo et al., and Gökhan [23] (L/h = 5, e = 0)

BCs	Theory	p					
		0	0.5	1	2	5	10
S-S	M. Turan [22]	5.2219	4.4692	4.0496	3.6936	3.4881	3.3643
	Nguyen et al. [48]	5.1528	4.4102	3.9904	3.6264	3.4009	3.2815
	Vo et al. [49]	5.1528	4.4019	3.9716	3.5979	3.3743	3.2653
	Gökhan [23]	5.1532	4.4016	3.9710	3.5970	3.3725	3.2644
	Outcome	5.1616	4.4189	3.9982	3.6323	3.4061	3.2874
C-C	M. Turan [22]	10.0864	8.7547	7.9841	7.2715	6.7148	6.3741
	Nguyen et al.[48]	10.0726	8.7463	7.9518	7.1776	6.4929	6.1650
	Vo et al. [49]	10.0678	8.7457	7.9522	7.1801	6.4961	6.1662
	Gökhan [23]	10.0321	8.7114	7.9200	7.1496	6.4626	6.1355
	Outcome	10.1575	8.8232	8.0187	7.2282	6.5384	6.2146
C-F	M. Turan [22]	1.9077	1.6286	1.4739	1.3446	1.2751	1.2636
	Nguyen et al. [48]	1.8957	1.6182	1.4636	1.3328	1.2594	1.2187
	Vo et al. [49]	1.8952	1.6180	1.4633	1.3326	1.2592	1.2184
	Gökhan [23]	1.8948	1.6176	1.4629	1.3322	1.2586	1.2178
	Outcome	1.9095	1.6301	1.4742	1.3422	1.2683	1.2274

Table 7. NFF of a beam for various porosity types, boundary conditions, e and p (L/h = 5)

Porosity	BCs	e	p					
			0	0.5	1	2	5	10
UP	S-S	0	5.1616	4.4189	3.9982	3.6323	3.4061	3.2874
		0.1	5.2357	4.4156	3.9176	3.4500	3.1545	3.0382
		0.2	5.3229	4.4073	3.7994	3.1589	2.7019	2.5817
		0.3	5.4272	4.3904	3.6160	2.6260	1.5250	1.1741
	C-C	0	10.1575	8.8232	8.0187	7.2282	6.5384	6.2146
		0.1	10.3183	8.8453	7.9022	6.9285	6.0814	5.7132
		0.2	10.5067	8.8625	7.7228	6.4418	5.2855	4.8330
		0.3	10.7309	8.8696	7.4286	5.5149	3.2345	2.3656
	C-F	0	1.9095	1.6301	1.4742	1.3422	1.2683	1.2274
		0.1	1.9336	1.6256	1.4409	1.2711	1.1727	1.1348
		0.2	1.9627	1.6194	1.3938	1.1595	1.0017	0.9656
		0.3	1.9983	1.6100	1.3227	0.9581	0.5575	0.4349
NUP-I	S-S	0	5.1616	4.4189	3.9982	3.6323	3.4061	3.2874
		0.1	5.2314	4.4642	4.0167	3.6142	3.3593	3.2411
		0.2	5.3065	4.5129	4.0346	3.5868	3.2884	3.1634
		0.3	5.3873	4.5653	4.0513	3.5461	3.1769	3.0173
	C-C	0	10.1575	8.8232	8.0187	7.2282	6.5384	6.2146
		0.1	10.2837	8.9026	8.0456	7.1749	6.3805	6.0177
		0.2	10.4183	8.9865	8.0693	7.0994	6.1517	5.7101
		0.3	10.5620	9.0752	8.0880	6.9925	5.8038	5.1754
	C-F	0	1.9095	1.6301	1.4742	1.3422	1.2683	1.2274
		0.1	1.9352	1.6468	1.4810	1.3360	1.2540	1.2152
		0.2	1.9629	1.6648	1.4877	1.3267	1.2322	1.1945
		0.3	1.9929	1.6843	1.4942	1.3129	1.1981	1.1562
NUP-II	S-S	0	5.1616	4.4189	3.9982	3.6323	3.4061	3.2874
		0.1	5.1733	4.3702	3.8936	3.4590	3.1924	3.0741
		0.2	5.1859	4.3118	3.7635	3.2297	2.8917	2.7743
		0.3	5.1996	4.2410	3.5973	2.9095	2.4230	2.2969
	C-C	0	10.1575	8.8232	8.0187	7.2282	6.5384	6.2146
		0.1	10.2091	8.7689	7.8681	6.9659	6.2170	5.8831
		0.2	10.2650	8.6990	7.6715	6.6033	5.7519	5.4103
		0.3	10.3259	8.6077	7.4059	6.0613	4.9790	4.6128
	C-F	0	1.9095	1.6301	1.4742	1.3422	1.2683	1.2274
		0.1	1.9101	1.6085	1.4317	1.2737	1.1839	1.1435
		0.2	1.9113	1.5835	1.3800	1.1846	1.0670	1.0270
		0.3	1.9130	1.5540	1.3153	1.0625	0.8879	0.8450

Table 8. NFF of a beam for various porosity types, boundary conditions, e and p (L/h = 10)

Porosity	BCs	e	p					
			0	**0.5**	**1**	**2**	**5**	**10**
UP	S-S	0	5.3959	4.6014	4.1608	3.7921	3.5950	3.4833
		0.1	5.4700	4.5933	4.0705	3.5941	3.3285	3.2271
		0.2	5.5577	4.5793	3.9400	3.2797	2.8452	2.7529
		0.3	5.6631	4.5557	3.7404	2.7093	1.5801	1.2389
	C-C	0	11.7576	10.0793	9.1274	8.2930	7.7537	7.4687
		0.1	11.9161	10.0648	8.9398	7.8784	7.1829	6.8971
		0.2	12.1055	10.0403	8.6694	7.2213	6.1661	5.8640
		0.3	12.335	9.9983	8.2540	6.0196	3.5166	2.7047
	C-F	0	1.9523	1.6635	1.5040	1.3716	1.3033	1.2638
		0.1	1.9762	1.6579	1.4689	1.2977	1.2050	1.1699
		0.2	2.0052	1.6505	1.4195	1.1819	1.0283	0.9977
		0.3	2.0409	1.6399	1.3454	0.9739	0.5684	0.4475
NUP-I	S-S	0	5.1616	4.6014	4.1608	3.7921	3.5950	3.4833
		0.1	5.2314	4.6510	4.1826	3.7776	3.5601	3.4566
		0.2	5.3065	4.7045	4.2043	3.7543	3.5057	3.4100
		0.3	5.3873	4.7624	4.2253	3.7185	3.4196	3.3235
	C-C	0	11.7576	10.0793	9.1274	8.2930	7.7537	7.4687
		0.1	11.9143	10.1807	9.1683	8.2509	7.6417	7.3520
		0.2	12.0829	10.2897	9.2080	8.1877	7.4725	7.1571
		0.3	12.2647	10.4072	9.2451	8.0947	7.2060	6.7906
	C-F	0	1.9523	1.6635	1.5040	1.3716	1.3033	1.2638
		0.1	1.9790	1.6809	1.5114	1.3661	1.2913	1.2555
		0.2	2.0079	1.6998	1.5189	1.3576	1.2728	1.2411
		0.3	2.0392	1.7204	1.5262	1.3448	1.2440	1.2154
NUP-II	S-S	0	5.3959	4.6014	4.1608	3.7921	3.5950	3.4833
		0.1	5.4019	4.5430	4.0425	3.5989	3.3555	3.2450
		0.2	5.4085	4.4742	3.8973	3.3466	3.0223	2.9131
		0.3	5.4159	4.3920	3.7146	3.0001	2.5120	2.3943
	C-C	0	11.7576	10.0793	9.1274	8.2930	7.7537	7.4687
		0.1	11.7749	9.9621	8.8857	7.8990	7.2729	6.9879
		0.2	11.7952	9.8241	8.5873	7.3799	6.5987	6.3155
		0.3	11.8190	9.6588	8.2082	6.6552	5.5462	5.2454
	C-F	0	1.9523	1.6635	1.5040	1.3716	1.3033	1.2638
		0.1	1.9517	1.6399	1.4589	1.2994	1.2140	1.1750
		0.2	1.9515	1.6128	1.4044	1.2062	1.0911	1.0526
		0.3	1.9518	1.5812	1.3367	1.0794	0.9048	0.8632

Table 9. NFF of a beam for various porosity types, boundary conditions, e and p (L/h = 20)

Porosity	BCs	e	p					
			0	**0.5**	**1**	**2**	**5**	**10**
UP	S-S	0	5.4610	4.6517	4.2056	3.8365	3.6488	3.5394
		0.1	5.5351	4.6421	4.1125	3.6340	3.3781	3.2816
		0.2	5.6228	4.6265	3.9785	3.3130	2.8860	2.8030
		0.3	5.7284	4.6010	3.7742	2.7319	1.5955	1.2578
	C-C	0	12.3090	10.5005	9.4972	8.6561	8.1997	7.9403
		0.1	12.4637	10.4702	9.2815	8.1970	7.5855	7.3481
		0.2	12.6505	10.4281	8.9763	7.4759	6.4829	6.2646
		0.3	12.8788	10.3659	8.5160	6.1754	3.6077	2.8285
	C-F	0	1.9637	1.6723	1.5119	1.3795	1.3127	1.2737
		0.1	1.9875	1.6665	1.4763	1.3047	1.2137	1.1794
		0.2	2.0165	1.6588	1.4263	1.1878	1.0355	1.0064
		0.3	2.0521	1.6477	1.3514	0.9780	0.5713	0.4509
NUP-I	S-S	0	5.4610	4.6517	4.2056	3.8365	3.6488	3.5394
		0.1	5.5380	4.7026	4.2284	3.8232	3.6178	3.5193
		0.2	5.6210	4.7575	4.2512	3.8013	3.5691	3.4834
		0.3	5.7108	4.8170	4.2735	3.7671	3.4921	3.4190
	C-C	0	12.3090	10.5005	9.4972	8.6561	8.1997	7.9403
		0.1	12.4774	10.6103	9.5440	8.6204	8.1165	7.8743
		0.2	12.6591	10.7292	9.5906	8.5651	7.9885	7.7606
		0.3	12.8559	10.8581	9.6359	8.4816	7.7870	7.5495
	C-F	0	1.9637	1.6723	1.5119	1.3795	1.3127	1.2737
		0.1	1.9907	1.6900	1.5195	1.3742	1.3014	1.2665
		0.2	2.0199	1.7091	1.5272	1.3659	1.2839	1.2540
		0.3	2.0516	1.7300	1.5347	1.3533	1.2567	1.2322
NUP-II	S-S	0	5.4610	4.6517	4.2056	3.8365	3.6488	3.5394
		0.1	5.4652	4.5905	4.0834	3.6376	3.4016	3.2936
		0.2	5.4701	4.5186	3.9337	3.3787	3.0589	2.9521
		0.3	5.4756	4.4331	3.7463	3.0245	2.5364	2.4211
	C-C	0	12.3090	10.5005	9.4972	8.6561	8.1997	7.9403
		0.1	12.3098	10.3572	9.2193	8.2094	7.6492	7.3925
		0.2	12.3135	10.1917	8.8816	7.6302	6.8884	6.6346
		0.3	12.3201	9.9972	8.4605	6.8389	5.7278	5.4555
	C-F	0	1.9637	1.6723	1.5119	1.3795	1.3127	1.2737
		0.1	1.9627	1.6482	1.4661	1.3062	1.2221	1.1835
		0.2	1.9622	1.6206	1.4108	1.2119	1.0976	1.0595
		0.3	1.9621	1.5883	1.3423	1.0839	0.9092	0.8681

4. Conclusions

The authors introduced a novel two-unknown model for analyzing the vibrations of FGP beams. The axial and transverse displacements of the beam are represented using a hybrid formula that integrates a series of polynomials and triangles. Using Lagrange's equations, it is possible to determine the defining equations of the FGP beams. Three varieties of boundary conditions and three types of porosity distributions were investigated in this study of beams. The efficacy of the proposed theory can be assessed using numerical examples. The boundary conditions, span-to-height ratio, power-law index, distribution type, and porosity coefficient were investigated. The results show that the suggested beam model is easy to use and good at predicting how FGP beams will vibrate when the boundary conditions and porosity distributions are changed.

Funding Statement

This research did not receive any specific grant from funding agencies in the public, commercial, or not-for-profit sectors.

Conflicts of Interest

The author declares that there is no conflict of interest regarding the publication of this article.

References

[1] Chen, D., Gao, K., Yang, J. and Zhang, L., 2023. Functionally graded porous structures: analyses, performances, and applications–a review. *Thin-Walled Structures*, 191, p.111046.

[2] Patel, P., Bhingole, P.P. and Makwana, D., 2018. Manufacturing, characterization and applications of lightweight metallic foams for structural applications. *Materials Today: Proceedings*, 5(9), pp.20391-20402.

[3] Maksoud, F.J., de la Paz, M.F.V., Hann, A.J., Thanarak, J., Reilly, G.C., Claeyssens, F., Green, N.H. and Zhang, Y.S., 2022. Porous biomaterials for tissue engineering: a review. *Journal of Materials Chemistry B*, 10(40), pp.8111-8165.

[4] Wu, H., Yang, J. and Kitipornchai, S., 2020. Mechanical analysis of functionally graded porous structures: A review. *International Journal of Structural Stability and Dynamics*, 20(13), p.2041015.

[5] Kiarasi, F., Babaei, M., Sarvi, P., Asemi, K., Hosseini, M. and Omidi Bidgoli, M., 2021. A review on functionally graded porous structures reinforced by graphene platelets. *Journal of Computational Applied Mechanics*, 52(4), pp.731-750.

[6] Nikbakht, S., Kamarian, S. and Shakeri, M., 2019. A review on optimization of composite structures Part II: Functionally graded materials. *Composite Structures*, 214, pp.83-102.

[7] Sayyad, A.S. and Ghugal, Y.M., 2019. Modeling and analysis of functionally graded sandwich beams: A review. *Mechanics of Advanced Materials and Structures*, 26(21), pp.1776-1795.

[8] Zhang, N., Khan, T., Guo, H., Shi, S., Zhong, W. and Zhang, W., 2019. Functionally graded materials: an overview of stability, buckling, and free vibration analysis. *Advances in Materials Science and Engineering*, 2019(1), p.1354150.

[9] Ameri, B., Moradi, M. and Talebitooti, R., 2021. Effect of honeycomb core on free vibration analysis of fiber metal laminate (FML) beams compared to conventional composites. *Composite Structures*, 261, p.113281.

[10] Najibi, A. and Shojaeefard, M.H., 2022. Fourier and time-phase-lag heat conduction analysis of the functionally graded porosity media. *International Communications in Heat and Mass Transfer*, 136, p.106183.

[11] Zarastvand, M.R., Ghassabi, M. and Talebitooti, R., 2022. Prediction of acoustic wave transmission features of the multilayered plate constructions: A review. *Journal of Sandwich Structures & Materials*, 24(1), pp.218-293.

[12] Talebitooti, R. and Zarastvand, M.R., 2018. The effect of nature of porous material on diffuse field acoustic transmission of the sandwich aerospace composite doubly curved shell. *Aerospace Science and Technology*, 78, pp.157-170.

[13] Zarastvand, M.R., Asadijafari, M.H. and Talebitooti, R., 2021. Improvement of the low-frequency sound insulation of the poroelastic aerospace constructions considering Pasternak elastic foundation.

Aerospace Science and Technology, 112, p.106620.

[14] Zarastvand, M.R., Ghassabi, M. and Talebitooti, R., 2021. A review approach for sound propagation prediction of plate constructions. *Archives of Computational Methods in Engineering*, 28, pp.2817-2843.

[15] Eltaher, M.A., Fouda, N., El-midany, T. and Sadoun, A.M., 2018. Modified porosity model in analysis of functionally graded porous nanobeams. *Journal of the Brazilian Society of Mechanical Sciences and Engineering*, 40, pp.1-10.

[16] Wattanasakulpong, N. and Ungbhakorn, V., 2014. Linear and nonlinear vibration analysis of elastically restrained ends FGM beams with porosities. *Aerospace Science and Technology*, 32(1), pp.111-120.

[17] Dang, V.H. and Nguyen, T.H., 2022. Buckling and nonlinear vibration of functionally graded porous micro-beam resting on elastic foundation. *Mechanics of Advanced Composite Structures*, 9(1), pp.75-88.

[18] Chen, D., Yang, J. and Kitipornchai, S., 2015. Elastic buckling and static bending of shear deformable functionally graded porous beam. *Composite Structures*, 133, pp.54-61.

[19] Kitipornchai, S., Chen, D. and Yang, J., 2017. Free vibration and elastic buckling of functionally graded porous beams reinforced by graphene platelets. *Materials & Design*, 116, pp.656-665.

[20] Zhao, J., Wang, Q., Deng, X., Choe, K., Xie, F. and Shuai, C., 2019. A modified series solution for free vibration analyses of moderately thick functionally graded porous (FGP) deep curved and straight beams. *Composites Part B: Engineering*, 165, pp.155-166.

[21] Van Vinh, P., Duoc, N.Q. and Phuong, N.D., 2022. A new enhanced first-order beam element based on neutral surface position for bending analysis of functionally graded porous beams. *Iranian Journal of Science and Technology, Transactions of Mechanical Engineering*, 46(4), pp.1141-1156.

[22] Turan, M., Uzun Yaylacı, E. and Yaylacı, M., 2023. Free vibration and buckling of functionally graded porous beams using analytical, finite element, and artificial neural network methods. *Archive of Applied Mechanics*, 93(4), pp.1351-1372.

[23] Adiyaman, G., 2024. Free vibration analysis of a porous 2D functionally graded beam using a high-order shear deformation theory. *Journal of Vibration Engineering & Technologies*, 12(2), pp.2499-2516.

[24] Eiadtrong, S., Wattanasakulpong, N. and Vo, T.P., 2023. Thermal vibration of functionally graded porous beams with classical and non-classical boundary conditions using a modified Fourier method. *Acta Mechanica, 234(2)*, pp.729-750.

[25] Askari, M., Brusa, E. and Delprete, C., 2021. On the vibration analysis of coupled transverse and shear piezoelectric functionally graded porous beams with higher-order theories. *The Journal of Strain Analysis for Engineering Design*, 56(1), pp.29-49.

[26] Nguyen, N.D., Nguyen, T.N., Nguyen, T.K. and Vo, T.P., 2022. A new two-variable shear deformation theory for bending, free vibration and buckling analysis of functionally graded porous beams. *Composite Structures*, 282, p.115095.

[27] Wattanasakulpong, N., Chaikittiratana, A. and Pornpeerakeat, S., 2018. Chebyshev collocation approach for vibration analysis of functionally graded porous beams based on third-order shear deformation theory. *Acta Mechanica Sinica*, 34, pp.1124-1135.

[28] Qin, B., Zhong, R., Wang, Q. and Zhao, X., 2020. A Jacobi-Ritz approach for FGP beams with arbitrary boundary conditions based on a higher-order shear deformation theory. *Composite Structures*, 247, p.112435.

[29] Shabani, Y., Mehdianfar, P. and Khorshidi, K., 2024. Static buckling and free vibration analysis of bi-dimensional FG metal ceramic porous beam. Mechanics of Advanced *Composite Structures*, 11(1), pp.149-158.

[30] Al Rjoub, Y.S. and Hamad, A.G., 2017. Free vibration of functionally Euler-Bernoulli and Timoshenko graded porous beams using the transfer matrix method. *KSCE Journal of Civil Engineering*, 21, pp.792-806.

[31] Anirudh, B., Ganapathi, M., Anant, C. and Polit, O., 2019. A comprehensive analysis of porous graphene-reinforced curved beams

by finite element approach using higher-order structural theory: Bending, vibration and buckling. *Composite Structures*, 222, p.110899.

[32] Wu, D., Liu, A., Huang, Y., Huang, Y., Pi, Y. and Gao, W., 2018. Dynamic analysis of functionally graded porous structures through finite element analysis. *Engineering Structures*, 165, pp.287-301.

[33] Mesbah, A., Belabed, Z., Amara, K., Tounsi, A., Bousahla, A.A. and Bourada, F., 2023. Formulation and evaluation a finite element model for free vibration and buckling behaviours of functionally graded porous (FGP) beams. *Structural Engineering and Mechanics,* vol. 86, p. 291.

[34] Turan, M. and Adiyaman, G., 2023. A new higher-order finite element for static analysis of two-directional functionally graded porous beams. *Arabian Journal for Science and Engineering*, 48(10), pp.13303-13321.

[35] Chen, D., Yang, J. and Kitipornchai, S., 2016. Free and forced vibrations of shear deformable functionally graded porous beams. *International journal of mechanical sciences*, 108, pp.14-22.

[36] Zhao, J., Wang, Q., Deng, X., Choe, K., Xie, F. and Shuai, C., 2019. A modified series solution for free vibration analyses of moderately thick functionally graded porous (FGP) deep curved and straight beams. *Composites Part B: Engineering*, 165, pp.155-166.

[37] Nguyen, N.D., Nguyen, T.N., Nguyen, T.K. and Vo, T.P., 2023, April. A Legendre-Ritz solution for bending, buckling and free vibration behaviours of porous beams resting on the elastic foundation. *In Structures*, Vol. 50, pp. 1934-1950. Elsevier.

[38] Hung, D.X., Truong, H.Q. and Tu, T.M., 2022. Nonlinear bending analysis of FG porous beams reinforced with graphene platelets under various boundary conditions by Ritz method. *In Modern Mechanics and Applications: Select Proceedings of ICOMMA 2020* (pp. 72-86). Springer Singapore.

[39] Sankar, B., 2001. An elasticity solution for functionally graded beams. *Composites Science and Technology,* 61(5), pp. 689-696.

[40] Yang, B., Ding, H.J. and Chen, W.Q., 2012. Elasticity solutions for functionally graded rectangular plates with two opposite edges simply supported. *Applied Mathematical Modelling*, 36(1), pp.488-503.

[41] Singh, A. and Kumari, P., 2018. Two-dimensional elasticity solution for arbitrarily supported axially functionally graded beams. *Journal of Solid Mechanics*, 10(4), pp.719-733.

[42] Wang, M., Xu, Y.G., Qiao, P. and Li, Z.M., 2019. A two-dimensional elasticity model for bending and free vibration analysis of laminated graphene-reinforced composite beams. *Composite Structures*, 211, pp.364-375.

[43] Wu, P., Yang, Z., Huang, X., Liu, W. and Fang, H., 2020. Exact solutions for multilayer functionally graded beams bonded by viscoelastic interlayer considering memory effect. *Composite Structures*, 249, p.112492.

[44] Serajzadeh, F. and Malekzadeh, P., 2023. Two-dimensional low-velocity impact analysis of curved sandwich beams with FG-CNTRC face sheets and porous core. *Mechanics Based Design of Structures and Machines*, 51(10), pp.5834-5855.

[45] Najibi, A., Kianifar, M. and Ghazifard, P., 2023. On the natural frequency investigation of the thick hollow cylinder with 2D-FGM Mori-Tanaka scheme. *Ships and Offshore Structures*, 18(12), pp.1638-1649.

[46] Najibi, A., Kianifar, M. and Ghazifard, P., 2023. Three-dimensional natural frequency investigation of bidirectional FG truncated thick hollow cone. *Engineering Computations*, 40(1), pp.100-125.

[47] Hadji, L., 2019. An analytical solution for bending and free vibration responses of functionally graded beams with porosities: Effect of the micromechanical models. *Structural Engineering and Mechanics, An Int'l Journal*, 69(2), pp.231-241.

[48] Nguyen, T.K., Nguyen, T.T.P., Vo, T.P. and Thai, H.T., 2015. Vibration and buckling analysis of functionally graded sandwich beams by a new higher-order shear deformation theory. *Composites Part B: Engineering*, 76, pp.273-285.

[49] Vo, T.P., Thai, H.T., Nguyen, T.K., Maheri, A. and Lee, J., 2014. Finite element model for vibration and buckling of functionally graded sandwich beams based on a refined shear deformation theory. *Engineering structures*, 64, pp.12-22.